Digital Robust Control Law Synthesis Using Constrained Optimization

Vivek Mukhopadhyay*
Planning Research Corporation, Inc., Hampton, Virginia

A direct digital control law synthesis procedure to meet multiple design requirements for a large-order flexible structure using the constrained optimization technique is described. A linear quadratic Gaussian-type cost function is minimized by updating the free parameters of the control law, while satisfying a set of constraints on the design loads, responses, and stability margins. Analytical expressions for gradients of the cost function and the constraints, with respect to the digital control law design variables, are used to facilitate rapid numerical convergence. The designer can choose the structure of the control law and the design variables, hence a stable classical control law as well as an estimator-based full- or reduced-order control law can be used as an initial starting point. Selected design responses can be treated as constraints instead of lumping them into the cost function. This feature was used to modify a control law in order to meet individual root-mean-square response limitations as well as minimum singular value restrictions. Low-order robust digital control laws were synthesized for gust-load alleviation of a flexible remotely piloted drone aircraft.

Nomenclature

A,B,C,D = control law quadruple matrices
$E[\ ]$ = expected value of $[\ ]$
F,G,H,E = plant quadruple matrices
g_n = nth constraint
G = plant transfer matrix
I = identity matrix
k = sampling stage
K = controller transfer matrix
M = order of control law
N_d = number of design output
N_s,N_c,N_o = order of plant, input, and output
N_g = number of constraints
N_w = number of plant noise input
$\hat{P}$ = control law matrix quadruple
R_u = noise covariance of η_k
R_v,R_w = noise covariance of v_k,w_k
$tr[\ ]$ = trace of a square matrix
T = sampling interval
u_k = plant input vector
v_k = output noise vector
w_k = plant noise vector
x_k = plant state vector
X,X_k = covariance of $\hat{x}_k$
y_k = plant output vector
y_{dk} = design output vector
δ_1,δ_2 = elevator, aileron deflections
δ_{kl} = Kroneker delta
η_k = fictitious input noise
Λ,Λ_k = Lagrange multiplier matrix
σ = minimum singular value
σ_D = desired minimum singular value

Received May 18, 1987; presented as Paper 87-2588 at the AIAA Guidance, Navigation, and Control Conference, Monterey, CA, Aug. 17-19, 1987; revision received Oct. 20, 1987.

*Associate Fellow, AIAA.

Introduction

A FLEXIBLE aircraft or space structure with active control is typically modeled by a large-order state space system of equations in order to accurately represent the rigid and flexible body modes, unsteady aerodynamic forces, actuator dynamics, and gust spectra.[1] The control law of this multi-input/multi-output (MIMO) system is expected to satisfy multiple design requirements on the dynamic loads, responses, actuator deflection, and rate limitations, as well as maintain certain stability margins, yet should be simple enough to be implemented on an onboard digital microprocessor. This paper describes a direct digital control law synthesis procedure for such a system, using the constrained optimization technique. The procedure minimizes a linear quadratic Gaussian (LQG) type cost function while trying to satisfy a set of contraints on the design loads, responses, and stability margins. Analytical expressions for the gradients of the cost function and the constraints, with respect to the control law design variables, are used for computation. This facilitates rapid convergence of the numerical optimization process. The designer can choose the structure of the control law and the design variables. This enables optimization of a classical control law as well as an estimator-based full- or reduced-order control law. Selected design responses are incorporated as inequality constraints instead of lumping them into the cost function. This feature is used to modify a control law to meet individual root-mean-square (rms) response limitations and design requirements. The minimum singular value of the return difference matrix at the plant input and output are also used as additional inequality constraints in order to improve the stability robustness properties in the frequency domain.

The basic gradient approach for synthesis of discrete control law of arbitrary order was proposed in Ref. 2. Additional formulation and optimization algorithms for output feedback system were presented in Refs. 3 and 4. The contribution of the present paper is 1) treatments of design requirements on rms loads and responses as inequality constraints, and 2) use of constraints on the minimum singular value to improve stability margins at the plant input and output. This procedure is the discrete-time equivalent of those presented in Refs. 1, 5, and 6 for a continuous-time system. Similar procedures, without the inequality constraints, were also presented in Refs. 7-10 in continuous-time domain. The

software developed to execute the present procedure can be used as a generic tool for parameter optimization of stable digital dynamic compensators. Second-order digital control laws were synthesized for gust-load alleviation of a remotely piloted flexible drone aircraft[11] that was modeled by a 32nd-order system. The stability robustness was improved at both the plant input and output.

System Description

A sampled data MIMO feedback control system can be modeled by a set of constant coefficient finite-difference equations in state space form as shown in Eqs. (1–5). They may represent discrete time, equations of motion, due to a small perturbation from a steady-state equilibrium condition for a flexible aircraft or a large space structure, and may be derived from the corresponding continuous equations.[1,12]

Plant

$$x_{k+1} = Fx_k + G_u(u_k + \eta_k) + G_w w_k \tag{1}$$

Output

$$y_k = Hx_k + v_k \tag{2}$$

Control law

$$z_{k+1} = Az_k + By_k \tag{3}$$

$$u_k = Cz_k + Dy_k \tag{4}$$

Design output

$$y_{dk} = H_d x_k + E_d u_k \tag{5}$$

where

$$k = 0,1,2,\ldots(N-1)$$

The plant state vector x_k, input vector u_k, plant disturbance w_k, plant output vector y_k, design output vector y_{dk}, and control law state vector z_k are of order N_s, N_c, N_w, N_o, N_d, and M, respectively. In general, the order of the control law M is lower than the order of the plant N_s. The plant disturbance w_k and output measurement error v_k are zero mean discrete white noise processes with covariance R_w and R_v, respectively. The vector η_k can be treated as a control command or as a fictitious plant input white noise process with covariance R_u.

$$E[w_k] = E[v_k] = E[\eta_k] = [0]$$

$$E[w_k w_l^T] = R_w \delta_{kl},\ E[v_k v_l^T] = R_v \delta_{kl}$$

$$E[\eta_k \eta_l^T] = R_u \delta_{kl} \tag{6}$$

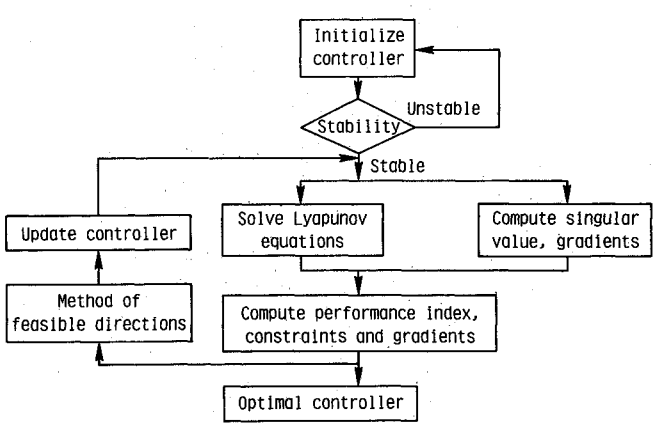

Fig. 1 Optimization scheme simplified block diagram.

Equations (1–4) may be expressed as an augmented system of equations, shown in Eqs. (7–9), which are similar to a simple output feedback formulation. Other variations of the augmented system formulation are possible depending on the controller structure.[4]

$$\begin{Bmatrix} x \\ z \end{Bmatrix}_{k+1} = \begin{bmatrix} F & 0 \\ 0 & 0 \end{bmatrix} \begin{Bmatrix} x \\ z \end{Bmatrix}_k + \begin{bmatrix} G_u & 0 \\ 0 & I \end{bmatrix} \begin{Bmatrix} u_k \\ z_{k+1} \end{Bmatrix} + \begin{bmatrix} G_u & G_w & 0 \\ 0 & 0 & 0 \end{bmatrix} \begin{Bmatrix} \eta_k \\ w_k \\ v_k \end{Bmatrix} \tag{7}$$

$$\begin{Bmatrix} y \\ z \end{Bmatrix}_k = \begin{bmatrix} H & 0 \\ 0 & I \end{bmatrix} \begin{Bmatrix} x \\ z \end{Bmatrix}_k + \begin{bmatrix} 0 & 0 & I \\ 0 & 0 & 0 \end{bmatrix} \begin{Bmatrix} \eta_k \\ w_k \\ v_k \end{Bmatrix} \tag{8}$$

$$\begin{Bmatrix} u_k \\ z_{k+1} \end{Bmatrix} = \begin{bmatrix} D & C \\ B & A \end{bmatrix} \begin{Bmatrix} y \\ z \end{Bmatrix}_k \tag{9}$$

Equations (7–9) may be rewritten in more familiar notation using a hat superscript to maintain the output feedback look. This simplifies the parameter optimization problem formulation and derivation of the gradient expressions considerably.

$$\hat{x}_{k+1} = \hat{F}\hat{x}_k + \hat{G}\hat{u}_k + \hat{G}_w\hat{\eta}_k \tag{10}$$

$$\hat{y}_k = \hat{H}\hat{x}_k + \hat{I}\hat{\eta}_k \tag{11}$$

$$\hat{u}_k = \hat{P}\hat{y}_k \tag{12}$$

Other forms of digital control laws, which include control input rates as additional states[4] or average delayed sampling[13] to account for computational delay (i.e., $z_{k+1} = Az_k + By_k + B_u u_k$ and $u_{k+1} = Cz_k + Dy_k + D_u u_k$ or $y_k = Hx_{k-1} + Eu_{k-1} + v_{k-1}$), can also be cast into the form of Eqs. (10–12).

Problem Formulation

A simplified block diagram of the constrained optimization scheme is shown in Fig. 1. For a given closed-loop stable system described by Eqs. (7–9) the free parameters of the controller quadruple $\hat{P}$ are updated in order to minimize the steady-state expected value of the cost function J defined by Eq. (13).

Cost function

$$J \equiv E\left[\begin{Bmatrix} \hat{x} \\ \hat{u} \end{Bmatrix}^T \begin{bmatrix} \hat{Q}_1 & \hat{M} \\ \hat{M}^T & \hat{Q}_2 \end{bmatrix} \begin{Bmatrix} \hat{x} \\ \hat{u} \end{Bmatrix} \right] \tag{13}$$

The minimization is subject to a set of inequality constraints on the steady-state mean-square values of selected design output responses defined by Eq. (14).

Constraints on the design output

$$g_n \equiv E[y_{d_n}^2]/E[y_{d_n\,\max}^2] - 1 \le 0 \qquad n = 1,2,\ldots,N_g \tag{14}$$

where $E[y_{d_n}^2]$ consists of selected diagonal terms of the matrix

$$E[y_d\, y_d^T] = [H_d\ E_d] E\left[\begin{Bmatrix} x \\ u \end{Bmatrix} \begin{Bmatrix} x \\ u \end{Bmatrix}^T \right] [H_d\ E_d]^T \tag{15}$$

In Eqs. (10–12), the subscript k has been dropped to indicate a stochastic steady-state condition and for clarity. Although the cost function J is defined in general terms, most of the design requirements can be imposed as inequality constraints in Eq. (14) instead of lumping them all in the cost function of

Eq. (13). This feature can be used to modify an existing control law to meet individual maximum rms response limitations and design requirements. Additional constraints are imposed on the minimum singular value σ of the return difference matrix at the plant input $[I + KG]$ and output $[I + GK]$, as shown in Eqs. (16) and (17), using the procedure reported in Ref. 6 for a continuous system. The transfer matrix of the plant $G(jw_pT)$ and compensator $K(\hat{P}, jw_pT)$ are defined in the frequency domain as $H[\exp(jw_p - T)I - F]^{-1}G_u$ and $C[\exp(jw_p - T)I - A]^{-1}B + D$, respectively, where T is the sampling period. The w_p is a set of N_p frequency points below the Nyquist frequency π/T radians.

Constraints on minimum singular value

$$g_{N_g} + 1(\hat{P}) \equiv \frac{1}{N_p} \sum_{p=1}^{N_p} [\max\{0, \sigma_D - \sigma[I + KG]\}]^2 \leq 0 \quad (16)$$

$$g_{N_g} + 2(\hat{P}) \equiv \frac{1}{N_p} \sum_{p=1}^{N_p} [\max\{0, \sigma_D - \sigma[I + GK]\}]^2 \leq 0 \quad (17)$$

The $\sigma_D(w_p)$ is the desired minimum singular value. Equations (16) and (17) provide a cumulative measure of violation of the singular value constraints. These constraints are usually imposed at a later stage of synthesis to improve stability robustness at the plant input and/or output. A graphical representation of these constraints is shown in Fig. 4 in Ref. 6. The idea is to reduce the area below the σ_D line to zero while keeping the system stable.

The analytical expressions for the gradients of the cost function and the constraints, with respect to the elements of the control law quadruple matrix $\hat{P}$, are described next. Using these gradients, a numerical constrained optimization technique called the method of feasible directions[14] is used to update the selected free parameters of the control law while attempting to satisfy the inequality constraints. The designer can choose the structure of the control law as well as the design variables. This enables optimization of classical control laws[15] as well as an estimator-based full- or reduced-order control laws.[13,16]

Gradients of the Cost Function

Substituting Eq. (12) into Eq. (10), the closed-loop system equations with white noise input may be written as

$$\hat{x}_{k+1} = F_a\hat{x}_k + G_a\hat{\eta}_k \quad (18)$$

where

$$F_a \equiv \hat{F} + \hat{G}\hat{P}\hat{H} \equiv \begin{bmatrix} F + G_uDH & G_uC \\ BH & A \end{bmatrix}$$

$$G_a \equiv \hat{G}_w + \hat{G}\hat{P}\hat{I} \equiv \begin{bmatrix} G_u & G_w & G_uD \\ 0 & 0 & B \end{bmatrix}$$

The steady-state mean-square responses can now be computed by solving for the steady-state condition of the discrete Lyapunov equation (19) that is satisfied by Eq. (18), since the augmented state vector and noise vector are uncorrelated and the expected values of their cross products are zero.[16,17]

$$X_{k+1} = F_aX_kF_k^T + G_aR_aG_a^T \quad (19)$$

Here $X_k = E[\hat{x}_k\hat{x}_k^T]$, and R_a is the square noise covariance matrix of $\hat{\eta}_k$. A steady-state solution will exist if the closed-loop system is stable (i.e., all eigenvalues of F_a have magnitudes less than unity). Once the steady-state value of X_k is known, the cost function and other mean-square responses can also be computed from Eqs. (10–12). After some matrix manipulation, the cost function in Eq. (13) can be expressed as

$$J = \text{tr}[\{Q_a + \hat{M}\hat{P}\hat{H} + (\hat{M}\hat{P}\hat{H})^T\}X] + \text{tr}[(\hat{P}\hat{I})^T\hat{Q}_2(\hat{P}\hat{I})R_a] \quad (20)$$

where

$$Q_a \equiv \hat{Q}_1 + (\hat{P}\hat{H})^T\hat{Q}_2(\hat{P}\hat{H})$$

The subscript k has been dropped to indicate a stochastic steady-state condition. Using a Lagrange multiplier matrix Λ_k and matrix trace properties, the gradients of the cost function J with respect to the elements of the matrix $\hat{P}$ can be expressed in a matrix form, as shown in Eq. (21). The derivation is similar to that presented in Ref. 1 for a continuous-time system.

$$\partial J/\partial\hat{P} = 2[(\hat{Q}_2 + \hat{G}^T\Lambda\hat{G})\hat{P}(\hat{H}X\hat{H}^T + \hat{I}R_a\hat{I}^T) + (\hat{G}^T\Lambda\hat{F} + \hat{M}^T)X\hat{H}^T] \quad (21)$$

Here X and Λ satisfy the steady-state condition of the discrete Lyapunov equations (19) and (22).

$$\Lambda_k = F_a^T\Lambda_{k+1}F_a + [Q_a + \hat{M}\hat{P}\hat{H} + (\hat{M}\hat{P}\hat{H})^T] \quad (22)$$

Equation (21) has exactly the same form as in the direct output feedback case,[4] and one can write explicit expressions for $\hat{P}$ by setting the gradient $\partial J/\partial\hat{P} = 0$. Starting from equations similar to Eqs. (19–22), explicit optimality conditions were derived by Bernstein et al.[13] In the present approach, the gradient expressions are used for numerical parameter search.

Gradients of the Design Output Constraints

The gradient of the constraints g_n, defined in Eq. 14 is obtained by deriving expressions for the gradients of selected diagonal terms in Eq. (15). This procedure is similar to that for the cost function gradient. For example, Eq. (15) can be written as

$$E[y_d\,y_d^T] = H_cXH_c^T + (E_dD)R_v(E_dD)^T \quad (23)$$

where

$$H_c = [H_d + E_dDH \vdots E_dC]$$

Assuming y_d to be a scalar y_{d_n} chosen as the nth constraint, and H_d and E_d to be the row vectors consisting of the nth row of the matrices H_d and E_d, respectively, one may write the scalar equation

$$E[y_d^2] = \text{tr}[H_c^TH_cX] + \text{tr}[(E_dD)^T(E_dD)R_v] \quad (24)$$

for each of the constraints, and the corresponding analytical gradient expressions are

$$\begin{aligned}
\partial E[y_d^2]/\partial A &= 2[\Lambda_c^*] \\
\partial E[y_d^2]/\partial B &= 2[(\Lambda_{sc}^TG_uD + \Lambda_cB)R_v + (\Lambda_{sc}^*H)^T] \\
\partial E[y_d^2]/\partial C &= 2[E_d^TE_d(DHX_{sc} + CX_c) \\
&\quad + E_d^TH_dX_{sc} + G_u^T\Lambda_{sc}^*] \\
\partial E[y_d^2]/\partial D &= 2[E_d^TE_d[(DHX_s + CX_{SC}^T)H^T + DR_v] \\
&\quad + E_d^TH_dX_sH^T + G_u^T[(\Lambda_sG_uD + \Lambda_{sc}B)R_v + \Lambda_s^*H^T]
\end{aligned} \quad (25)$$

where

$$\Lambda^* \equiv \Lambda F_aX \equiv \begin{bmatrix} \Lambda_s^* & \Lambda_{sc}^* \\ \Lambda_{sc} & \Lambda_c^* \end{bmatrix}_{(N_s+M)\times(N_s+M)} \quad (26)$$

$$X \equiv \begin{bmatrix} X_s & X_{sc} \\ X_{sc}^T & X_c \end{bmatrix}_{(N_s+M)\times(N_s+M)} \quad (27)$$

and X and Λ satisfy the steady-state condition of the discrete Lyapunov equations (19) and (28).

$$\Lambda_k = F_a^T \Lambda_{k+1} F_a + [H_c^T H_c] \tag{28}$$

The gradients of the singular value constraints defined in Eqs. (16) and (17) were derived as in the continuous-time case.[18,19]

Design Variables

Since all the elements of the control law quadruple matrices A, B, C, and D in Eqs. (3) and (4) are not independent, it is necessary to choose a set of design variables from the $M(N_o + N_c) + N_o N_c$ free elements.[1,7] There are several possible ways of doing this. For a transfer function type control law in the Z or ω domain,[16] the variable elements can be identified. If Eqs. (3) and (4) are expressed in block diagonal form or in minimum realization form, the nonzero elements of the A matrix can be identified as the real and imaginary part of the compensator eigenvalues. The elements of matrix C can be treated as feedback gains and can be used as design variables. This approach was used for the design example. In the digital control law synthesis software, the designer initially selects a set of design variables from the elements of the matrix $\hat{P}$. The elements that do not change substantially over the iteration, or have relatively small normalized gradients, can later be eliminated. Starting with a stable control law and using the optimization scheme shown in Fig. 1, the design variables can be modified to minimize the cost function and satisfy the design constraints.

Gust Load Alleviation Example

The parameter optimization procedure was applied to synthesize second-order digital control laws for gust-load alleviation (GLA) of the flexible drone aircraft reported in Refs.5 and 11. The basic control scheme is shown in Fig. 2. In longitudinal motion, the symmetric elevator and outboard aileron deflections are used as the two control inputs. Accelerometer sensors positioned symmetrically near outboard ailerons and in the fuselage near the center of gravity are used as two measurement outputs. The linear, small-pertubation equations of motion of the flexible aircraft in longitudinal, symmetric level flight was expressed by a 19th-order

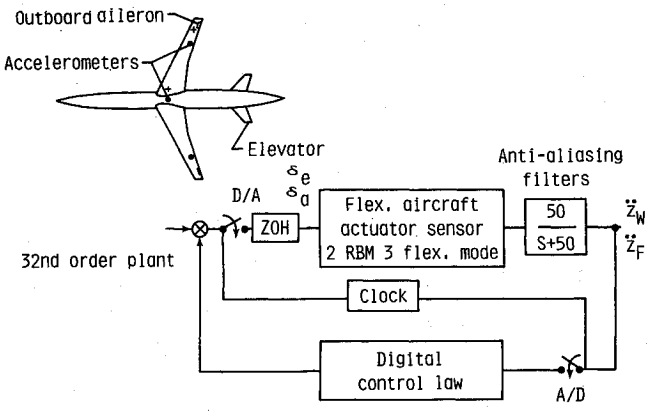

Fig. 2 Gust-load alleviation control scheme.

state space system of equations. This basic model included rigid body plunge rate, pitch, pitch rate, three wing flexible modes, and two aerodynamic lag terms[1,9] for each of the rigid and flexible modes. These lag terms are used to model the unsteady aerodynamic effects, approximately. The rigid body plunge position mode was excluded, since it does not contribute to the dynamics. A third-order elevator actuator dynamics [20/(s + 20) with a 100 Hz double-pole filter] and an eighth-order aileron actuator dynamics were added. A second-order filter, shown in Eq. (29), which approximates the Dryden gust spectrum driven by a unit white noise w to generate a 1 in./s rms transverse gust velocity, was also added to obtain a 32nd-order continuous plant model. (Details of the continuous and discrete models, with sampling at 100 Hz, are available from the author.)

$$\frac{\xi_g}{w} = \sigma_{wg}\sqrt{3V/l}\,[(V/l\sqrt{3}) + s)]/[(V/l) + s]^2 \tag{29}$$

Here ξ_g is the gust state, σ_{wg} the rms gust velocity, l the scale of turbulence or characteristic length, and V the flight velocity. For numerical calculation, the design flight condition was chosen at 24,000 ft altitude, at dynamic pressure of 2.95 psi, and l = 2500 ft. The corresponding flight velocity was 10,530 in./s, and Mach number was 0.86. The open-loop eigenvalues corresponding to the plunge, pitch, and three wing flexure modes were -1.466, $-0.1346 \pm j5.468$, $-13.4 \pm j86.89$, $-32.43 \pm j168.6$, and $-14.05 \pm j218.8$, respectively. Design responses, such as wing root bending moment (WRBM) and wing root shear (WRS), wing outboard bending moment (WOBM) and wing outboard torsion (WOT), symmetric elevator and aileron deflections and rate, were computed.

The objective was to design a robust, low-order, digital GLA control law, which will reduce by half the open-loop rms values of the wing root bending moment and shear without increasing the rms outboard bending moment and torsion to aviod shifting the wing load outboard. The robustness requirement was specified in terms of minimum singular value of the return difference matrix at the plant input and output. A minimum value of $\sigma_D = 0.6$ would provide a simultaneous guaranteed MIMO gain or phase margins of -4 dB, $+8$ dB, or ± 35 deg, respectively.[6,18]

GLA Control Law Synthesis

The open-loop rms values of WRBM, WRS, WOBM, and WOT were obtained first by solving the steady-state Lyapunov equation. These were found to be 209.6 lb-in, 3.75 lb, 1.66 lb-in, and 0.76 lb-in, respectively, for a 1 in./s rms gust. The maximum allowable rms deflection and rate for the elevator and aileron were specified to be 0.00006981 rad, 0.0035 rad/s, 0.000412 rad, and 0.0558 rad/s, respectively, for a 1 in./s rms Dryden gust. Second-order digital GLA control laws were synthesized to meet the design objectives and were compared with full-order LQG control laws. A summary of the result obtained is presented in Tables 1-3. The rms wing loads, as percentages of the corresponding open-loop values for different control laws, are presented in Table 1. The control surface

Table 1 Root-mean-square wing loads as percentages of open-loop values, and control surface activities as percentages of maximum allowed due to a unit rms gust

	rms loads on wing due to unit Dryden gust, % of open loop				rms control deflection and rate, % of maximum allowed			
	Wing root		Wing outboard		Elevator		Aileron	
Design (order)	BM	Shear	BM	Torsion	δ_1	$\dot{\delta}_1$	δ_2	$\dot{\delta}_2$
Open loop	100	100	100	100	0	0	0	0
Full state	26	25	23	17	49	6	35	32
LQG (32)	49	49	81	57	20	3	13	9
Law I (2)	63	60	140	63	13	1.5	51	10
Law II (2)	43	43	101	66	25	1.7	25	1.3
Law III (2)	45	45	92	62	33	3	5	1
Law IV (2)	46	46	93	63	27	3	2	1

Table 2 Peak time responses of WRBM, WRS, WOBM, WOT, elevator and aileron deflections, short-period frequency, and damping ratio, due to a 1 in./s step-gust input

Design (order)	WRBM, lb-in.	WRS, lb	WOBM, lb-in.	WOT, lb-in.	δ_1, rad $\times 10^{-4}$	δ_2 rad $\times 10^{-4}$	ω_{sp}, rad/s	ζ_{sp},
Open-loop	36	0.65	0.12	0.10	0	0	6.47	0.017
Full state	20	0.35	0.09	0.06	0.25	0.13	7.04	0.430
LQG (32)	32	0.58	0.12	0.08	0.29	0.30	5.50	0.170
Law I (2)	32	0.55	0.28	0.05	0.04	0.40	5.86	0.060
Law II (2)	30	0.55	0.26	0.12	0.05	0.46	5.82	0.175
Law III (2)	28	0.52	0.12	0.07	0.16	0.16	5.75	0.136
Law IV (2)	32	0.58	0.12	0.07	0.08	0.025	5.49	0.179

Table 3 Second-order digital control law quadruples for gust-load alleviation

Law I

$$A = \begin{bmatrix} 0.9621 & 0 \\ 0 & 0.8706 \end{bmatrix} \quad C = \begin{bmatrix} -0.00141 & -0.00179 \\ -0.01196 & -0.0405 \end{bmatrix}$$

Law II

$$A = \begin{bmatrix} 0.9712 & 0 \\ 0 & 0.8646 \end{bmatrix} \quad C = \begin{bmatrix} -0.00201 & -0.00077 \\ -0.01424 & -0.01278 \end{bmatrix}$$

Law III

$$A = \begin{bmatrix} 0.9933 & 0 \\ 0 & 0.9944 \end{bmatrix} \quad C = \begin{bmatrix} -0.00245 & -0.00071 \\ -0.01531 & -0.01117 \end{bmatrix}$$

Law IV

$$A = \begin{bmatrix} 0.9698 & 0 \\ 0 & 0.9721 \end{bmatrix} \quad C = \begin{bmatrix} -0.00270 & -0.00068 \\ -0.01512 & -0.01133 \end{bmatrix}$$

All

$$B = \begin{bmatrix} 0.000208 & 0.000444 \\ -0.000263 & -0.000578 \end{bmatrix} \quad D = \begin{bmatrix} 0 & 0 \\ 0 & 0 \end{bmatrix}$$

rms deflections and rate, as percentages of maximum allowable values, are also shown in Table 1. The peak transient loads and responses due to a 1 in./s step gust input for the open-loop system and the closed-loop system with different control laws are presented in Table 2. The short period frequency and damping ratios are also shown in Table 2. The second-order digital control law quadruples are shown in Table 3.

In order to obtain a stable initial control law, it was convenient to start with a continuous system, obtain a state feedback controller and a LQG state estimator, and then reduce the order of the resulting LQG control law by truncation or residualization.[1,12] The reduced-order controller in block diagonal form was then discretized, using Z transform with a zero-order hold and a sampling rate of 100 Hz. Two $50/(s + 50)$ anti-aliasing filters were added to the two accelerometer measurements of the continuous plant model. The plant state space model was then discretized, using Z transform with a zero-order hold at 100 Hz sampling rate. Unconstrained and constrained optimization schemes were applied on these discrete models of plant and control laws.

Full-Order LQG Control Laws

A state feedback optimal GLA control law for the continuous-time system was obtained using $J \equiv E[y_d^T Q_1 y_d + u^T Q_2 u]$ where y_d consisted of WRBM, WRS, WOBM, and WOT, and u consisted of elevator and aileron input δ_1 and δ_2, respectively. The diagonal weighting matrix Q_1 was chosen as the inverse of maximum desired mean-square value of the WRBM, WRS, WOBM, and WOT (i.e., $Q_1 = \text{diag}\,[1/(104.8)^2\ 1/(1.87)^2\ 1/(1.66)^2\ 1/(0.76)^2]$). The diagonal weighting matrix Q_2 was also chosen as the inverse of maximum allowable mean-square elevator and aileron deflections, following Bryson's rule[17] ($Q_2 = \text{diag}\,[1/(0.00006981)^2\ 1/(0.0035)^2]$). The corresponding rms values due to a 1 in./s rms gust are shown in Table 1 as percentages of open-loop responses for the wing loads and as percentages of maximum allowable deflection and rate for the control surfaces. The peak transient loads and control surface deflections for the full-state design, due to a 1 in./s step gust input are shown in Table 2. The corresponding short period damping ratio is 0.43.

This full-state LQ control law satisfies all the design requirements, but it cannot be implemented since all the states are not available for feedback. The implementation may be possible with an LQG state estimator. This was designed using $R_u = [0]$, $R_w = 1$ (a unit intensity plant noise input, corresponding to a 1 in./s rms Dryden gust), and measurement noise intensity $R_v = \text{diag}\,[2\ 1]$ for the wing and fuselage acceleration measurements, respectively. The closed-loop normalized rms responses using the 32nd-order LQG state estimator are higher, as expected, compared to the full-state case, but they still satisfy the design requirements. This is shown in Table 1, where all the rms values were computed assuming zero measurement noise. The peak transient loads due to a unit step gust input increased considerably, as shown in Table 2. The corresponding short period damping was reduced to 0.170.

Second-Order GLA Control Laws

Initial Control Law (Law I)

The 32nd-order LQG control law is difficult to implement in a flight computer. A low-order control law with similar performance is often desirable. It was found that a stable second-order control law can be obtained by truncating the full-order LQG control law, retaining only the key controller states corresponding to the pitch angle and pitch rate perturbation state estimates.[1,9] This second-order control law was transformed into a block diagonal form and then discretized using Z transform with a zero-order hold at 100 samples/s. The results are shown in Table 3 as Law I. This truncated control law was stable, and the corresponding normalized rms values of the closed-loop sampled data system, using discrete plant input noise intensity R_w of $1/T$ (corresponding to approximately 1 in./s rms Dryden gust), is shown in Table 1. Although the rms values of WRBM, WRS, and WOT were reduced by 30% the WOBM increased over 40%, and none of the design requirements were satisfied. The aileron rms deflections increased considerably but were still within the allowable limits. The short period damping ratio was only 0.060 (see Table 2).

Unconstrained Optimization (Law II)

The present optimization procedure was applied next, using Law I as the initial value in order to satisfy the design requirements. First, the unconstrained optimization was attempted, using the same weighting matrices on the design output and control input as in the full-state continuous case. A unit rms gust was used to drive the system, and the measurement noises were set to zero. The four elements of the C matrices and the diagonal elements of the A matrix were used as the six design variables. The optimized control law obtained after five iterations is shown in Table 3 as Law II. The corresponding closed-loop normalized rms responses, shown in Table 1, indicate 57% reduction in the WRBM and WRS and 37% reduction in WOT. The WOBM, however, was 1% higher than the corresponding open-loop value. The rms

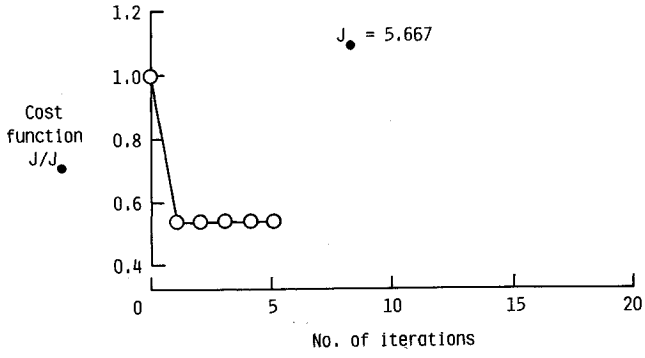

Fig. 3 Normalized cost function vs iteration (unconstrained optimization, Law II).

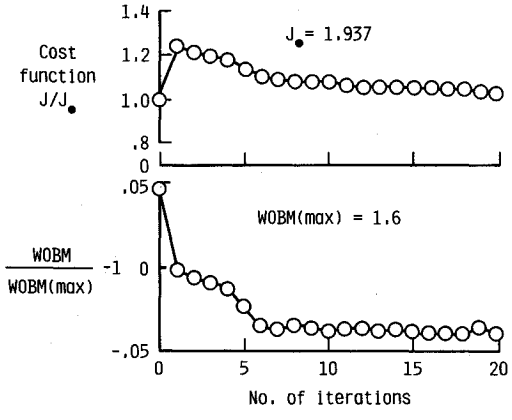

Fig. 4 Normalized cost function and constraint vs iteration (constrained optimization, Law III).

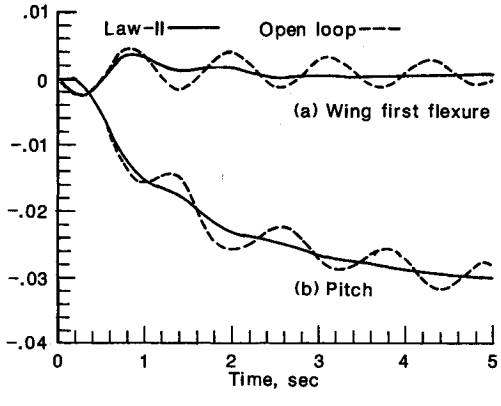

Fig. 5 Time responses of a) first wing flexure mode, b) pitch mode due to 1 in./s step gust.

control surface activities indicate equal sharing of workload by the elevator and aileron. The short period damping ratio was about 0.175. The plot of normalized cost function vs number of iterations, shown in Fig. 3, indicates convergence in one iteration.

Constrained Optimization (Law III)

In order to prevent the small increase in the outboard bending moment, the constrained optimization procedure was attempted next, using the control Law II as the initial value. The rms outboard bending moment was treated as a constraint, instead of lumping it with the cost function. The maximum allowable rms value of WOBM was chosen as 1.6. After 20 iterations, an optimized control law was obtained. It is designated as Law III and is shown in Table 3. The corresponding closed-loop rms values, shown in Table 1, indicate net reduction in the open-loop WRBM, WRS,

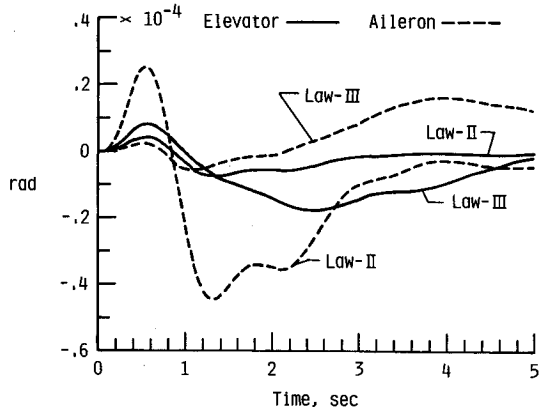

Fig. 6 Time responses of elevator and aileron deflections due to 1 in./s step gust.

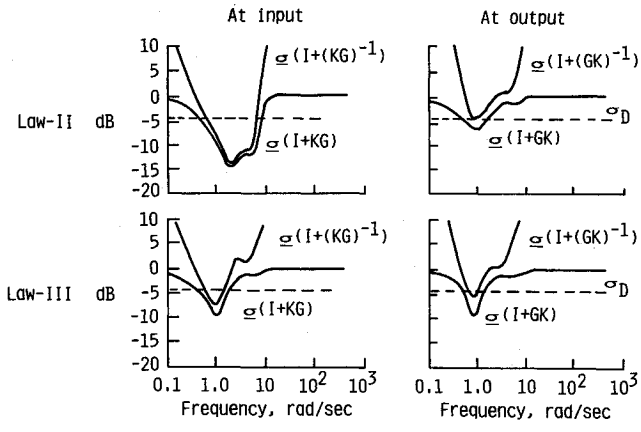

Fig. 7 Minimum singular value plots at plant input and output (Law II and Law III).

WOBM, and WOT by 55, 55, 8, and 38%, respectively. The rms control surface activities indicate that most of the workload was shifted to the elevator. The peak transient loads were lower compared to Law II, although the short period damping ratio was reduced to 0.136 (Table 2). The plot of cost function and constraint vs iteration, shown in Fig. 4, indicates that the constraint on WOBM was satisfied in one iteration at the expense of increased cost function, which was subsequently reduced along with the WOBM.

The transient responses of the open-loop system and the closed-loop system with Law II for a 1 in./s step gust is shown in Fig. 5 for the first wing flexure mode and pitch mode. The GLA control Law II damped out the transients in about 2.5 s. In order to compare the transient response characteristics of the different control laws, the peak transient responses are tabulated in Table 2. The transient responses of the elevator and aileron deflections of the closed-loop system, using Laws II and III, are shown in Fig. 6. From Table 2 and Fig. 6, Law III appears to provide better transient response to a unit step gust than Law II.

Stability Margin Improvement (Law IV)

The stability margins at the plant input and output were evaluated by computing the minimum singular values of the corresponding return difference and inverse return difference matrices, as in the continuous-time case.[6,18,19] For the discrete system, the singular values were computed by replacing the term Z in the Z domain transfer matrix with $\exp(jw_pT)$, where w_p is a set of N_p frequency points below the Nyquist frequency π/T, and T is the sampling period.[12] The input and output signals were assumed to coincide with the sampling instant. The minimum singular value plots of the return difference matrix and inverse return difference matrix at the plant input and output using Laws II and III are shown in Fig. 7. At the

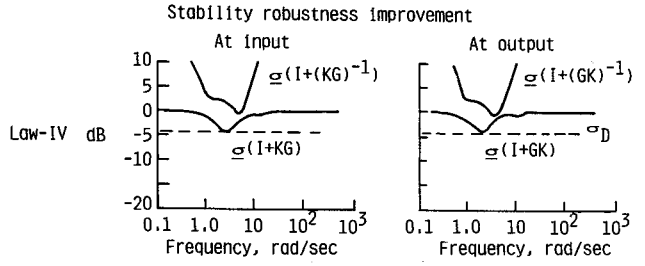

Fig. 8 Optimized minimum singular value plots at plant input and output (Law IV).

plant input, the minimum singular values of $(I + KG)$ and $[I + (KG)^{-1}]$ were -15.0 and -14.5 dB, respectively, for Law II and -10.0 and -7.5 dB, respectively, for Law III. The corresponding maximum guaranteed simultaneous gain or phase margins at the plant input were $+1.8$ dB, -1.9 dB, or ± 12 deg for Law II, and $+3.4$ dB, -4.8 dB, or ± 24 deg for Law III, respectively. At the plant output, the minimum singular values of $(I + GK)$ and $[I + (GK)^{-1}]$ were -7.0 and -5.0 dB, respectively, for Law II and -9.0 and -5.6 dB, respectively, for Law III. These values correspond to gain or phase margins of $+5$ dB, -7 dB, or ± 33 deg for Law II, and $+3.8$ dB, -6 dB, or ± 30 deg for Law III, respectively. From the singular value analysis, Laws II and III appear to be robust to perturbations at plant output but not at plant input.

In order to improve stability robustness at both the plant input and output, Law III was re-optimized using two additional constraints corresponding to a required minimum singular value of $(I + KG)$ and $(I + GK)$ not less than 0.6 or -4.43 dB, as shown by the dashed lines in Fig. 7. The constraint on the wing outboard bending moment was also retained. After seven iterations, an optimized control law was obtained. It is designated as Law IV and is shown in Table 3. The corresponding closed-loop rms loads and peak transient responses increased marginally from those of Law III and are presented in Tables 1 and 2. The minimum singular value plots at the plant input and output are shown in Fig. 8. At the plant input, the minimum singular values of $(I + KG)$ and $[(I + KG)^{-1}]$ were -4.63 and -1.0 dB, respectively, for Law IV. These correspond to maximum gain or phase margins of $+5.5$ dB, -16 dB, or ± 53 deg, respectively, at the plant input. At the plant output, the minimum singular values of $(I + GK)$ and $[I + (GK)^{-1}]$ were -4.56 and -0.9 dB, respectively, for Law IV. These values correspond to gain or phase margins of $+5.7$ dB, -17 dB, or ± 53 deg for Law IV, respectively, at the plant output. Thus, substantial improvement in stability robustness was obtained at the plant input and output by using the constrained optimization technique.

Conclusions

A generic procedure for parameter optimization of a digital control law for a large-order flexible flight vehicle or large space structure modeled as a sampled data system was presented. A linear quadratic Gaussian-type cost function was minimized while satisfying a set of constraints on the steady-state root-mean-square values of selected design loads and responses and on minimum singular values, using a constrained optimization technique to meet multiple design requirements. Analytical expressions for the gradients of the cost function and the design constraints on mean-square responses with respect to the control law design variables were presented. This type of gradient computation seemed to facilitate fast convergence of the numerical optimization process. The methodology can be used to optimize a digital control law synthesized by classical methods or an estimator-based full- or reduced-order control law. The effects of anti-aliasing filters and other delay terms can be included in the design process. Existing control laws can be modified to meet individual response limitations and design requirements.

The synthesis methodology was demonstrated using a gust-load alleviation problem of a drone aircraft modeled by a 32nd-order system. Second-order digital gust-load alleviation control laws were synthesized and compared with full-order optimal control laws. The low-order digital control law reduced the open-loop rms values of the wing root bending moment and shear by 55% without increasing the outboard bending moment due to a random Dryden gust. The wing outboard torsion was reduced by 38%. The control surface deflections and rate were within the allowable limits. The stability margins were evaluated from the singular value analysis and then improved at the plant input and output by satisfying singular value constraints.

Acknowledgments

The research support through NASA Langley Contract NAS1-18000 and technical discussion with research monitors Jerry Newsom and Mike Gilbert are gratefully acknowledged.

References

[1]Mukhopadhyay, V., Newsom, J.R., and Abel, I., "A Method for Obtaining Reduced Order Control Laws for High Order Systems Using Optimization Technique," NASA TP-1876, Aug. 1981.

[2]Kwakernaak, K. and Sivan, R., *Linear Optimal Control Systems*, Wiley, New York, 1972, pp. 552-554.

[3]Joshi, S.M., "Design of Optimal Partial State Feedback Controllers for Linear Systems in Stochastic Environment," NASA TM-X-72203, Aug. 1974.

[4]Halyo, N. and Broussard, J.R., "Investigation Development and Application of Optimal Output Feedback Theory," NASA CR-3828 (NAS1-15759), Aug. 1984.

[5]Newsom, J.R. and Mukhopadhyay, V., "Application of Constrained Optimization to Active Control of Aeroelastic Response," NASA TM-83150, June 1981.

[6]Mukhopadhyay, V., "Stability Robustness Improvement Using Constrainted Optimization Techniques," *Journal of Guidance, Control, and Dynamics*, Vol. 10, March-April 1987, pp. 172-177.

[7]Martin, G.D. and Bryson, A.E., Jr., "Attitude Control of Flexible Spacecraft," *Journal of Guidance, Control, and Dynamics*, Vol. 3, Jan.-Feb. 1980, pp. 37-41.

[8]Gangsaas, D. and Ly, U.-L, "Practical Gust Load Alleviation and Flutter Suppression Control Laws Based on LQG Methodology," AIAA Paper 81-0021, Jan. 1981.

[9]Mukhopadhyay, V., Newsom, J.R., and Abel, I., "Reduced Order Feedback Control Law Synthesis for Flutter Suppression," *Journal of Guidance, Control, and Dynamics*, Vol. 5, July-Aug. 1982, pp. 389-395.

[10]Ly, U.-L, "Design Algorithm for Robust Low Order Controllers," Department of Aeronautics and Astronautics, Stanford University, Stanford, CA, SUDAAR Rept. 536, Nov. 1982.

[11]Murrow, H.N. and Eckstrom, C.V., "Drone for Aerodynamic and Structural Testing (DAST), A Status Report," *Journal of Aircraft*, Vol. 16, Aug. 1979, pp. 521-526.

[12]Mahesh, J.K., Ward, W.M., and Konar, A.F., "Interactive Flight Control System Analysis Program," Vol. II, DIGIKON IV User Reference Manual, NASA CR-NAS1-164438 Nov. 1983.

[13]Bernstein, D.E., Davis, L.E., and Greeley, S.W., "The Optimal Projection Equations For Fixed-order Sampled Data Dynamic Compensation with Computation Delay," *IEEE Transactions on Automatic Control*, Vol. AC-31, Sept. 1986, pp. 859-862.

[14]Vanderplatts, G.N., "CONMIN-A Fortran Program for Constrained Function Minimization-User Manual," NASA TM X-62282, Aug. 1973.

[15]Ruer, D., Whitbeck, R.F., and Magdaleno, R.E., "Methodologies for the Direct Digital Control of Highly Flexible Vehicles," Air Force Wright Aeronautical Lab., AFWAL-TR-84-3104, Feb. 1985.

[16]Franklin, D.F. and Powell, D., *Digital Control of Dynamic Systems*, Addison-Wesley, Reading, MA 1980, pp. 260-262.

[17]Bryson, A.E., Jr. and Ho, Y.C., *Applied Optimal Control*, Hemisphere, Washington DC, 1975, pp. 360-362.

[18]Mukhopadhyay, V. and Newsom, J.R., "A Multiloop System Stability Margin Study Using Matrix Singular Values," *Journal of Guidance, Control, and Dynamics*, Vol. 7, Sept.-Oct. 1984, pp. 582-587.

[19]Newsom, J.R. and Mukhopadhyay, V., "A Multiloop Robust Controller Design Study Using Singular Value Gradients," *Journal of Guidance, Control, and Dynamics*, Vol. 4, July-Aug. 1985, pp. 514-519.